

Simple-source model of military jet aircraft noise^{1),2),3)}

Jessica Morgan^{a)}, Tracianne B. Neilsen^{b)}, Kent L. Gee^{c)}, Alan T. Wall^{d)} and Michael M. James^{e)}

(Received: 14 February 2012; Revised: 3 July 2012; Accepted: 3 July 2012)

This paper describes a method for determining a semi-empirical, equivalent simple-source model that accounts for the sound radiation in the vicinity of a high-performance military aircraft. The characteristics of the equivalent source are guided by previously reported observations of jet noise, namely that the strengths of the partially correlated sources are distributed asymmetrically. The parameters of the equivalent source model are chosen to reproduce the data recorded on large planar apertures in the near-field of an F-22 Raptor. First, the location of the dominant source region for a given frequency is found by matching the orientation of the interference nulls in a sound pressure level map. Second, the relative contributions of the correlated and uncorrelated portions of the equivalent source are chosen to replicate the directionality and extent of the sound field. The source characteristics are selected based on the data at one measurement plane but are able to approximate the radiation at other near- and mid-field locations. The method is used to find equivalent sources at several frequencies and different engine conditions. © 2012 Institute of Noise Control Engineering.

Primary subject classification: 13.1.5; Secondary subject classification: 21.6.1

¹⁾ SBIR DATA RIGHTS—(DFARS 252.227-7018 (JUNE 1995)); Contract Number: FA8650-08-C-6843; Contractor Name and Address: Blue Ridge Research and Consulting, LLC, 15 W Walnut St. Suite C; Asheville, NC. Expiration of SBIR Data Rights Period: March 17, 2016 (subject to SBA SBIR Directive of September 24, 2002). The government's rights to use, modify, reproduce, release, perform, display, or disclose technical data or computer software marked with this legend are restricted during the period shown as provided in paragraph (b)(4) of the Rights in Noncommercial Technical Data and Computer Software—Small Business Innovation Research (SBIR) Program clause contained in the above identified contract. No restrictions apply after the expiration date shown above. Any reproduction of technical data, computer software, or portions thereof marked with this legend must also reproduce the markings.

²⁾ Distribution A – Approved for public release; Distribution is unlimited 88ABW-2012.0563.

³⁾ This is the sixth paper published in NCEJ on the special issue of Military Noise.

^{a)} Department of Physics and Astronomy, Brigham Young University, Provo UT USA.

^{b)} Department of Physics and Astronomy, Brigham Young University, Provo UT USA; email: tbn@byu.edu.

^{c)} Department of Physics and Astronomy, Brigham Young University, Provo UT USA; email: kentgee@byu.edu.

^{d)} Department of Physics and Astronomy, Brigham Young University, Provo UT USA; email: alantwall@gmail.com.

^{e)} Blue Ridge Research and Consulting LLC, 15 W. Walnut Street, Asheville NC USA.

1 INTRODUCTION

This paper describes the development of an equivalent source model (ESM) using simple sources to predict the radiation of jet noise produced by military jet aircraft. Development of such a model has at least two benefits. First, the near-aircraft environment can be predicted, which is beneficial in establishing auditory risk for, e.g., flight crew personnel working on an aircraft carrier deck. Second, an ESM can be evaluated in a computationally efficient manner, which allows the effects of individual parameters to be examined. Though the ESM is not directly tied to physical radiation mechanisms, parametric studies can yield information about which variables are correlated with significant changes in radiation. This could point to directions for more direct source-related research.

Although some researchers have been able to probe jet turbulence for important features (e.g., see Refs. 1 and 2), the heated, supersonic flow present in high-power military jet aircraft engine plumes has thus far precluded such direct investigations. Information about the source properties can be extracted, however, by comparing the predictions of acoustic modeling with the measured noise. Although significant progress continues to be made on various fronts in computational aeroacoustics modeling, analytical (e.g., see Refs. 3 and 4) and empirical (e.g., see Refs. 5–7) acoustical models play an important role in efficiently

understanding the relevant physics of the noise sources and radiation. Some modeling techniques, such as near-field acoustical holography,⁸⁻¹⁰ begin with measured data and then rely on an analytical propagation model to estimate the sound field elsewhere.

An ESM is also a data-based source characterization method¹¹ that uses some *a priori* knowledge of, or assumption regarding, the source characteristics¹². From this assumption, a distribution of equivalent sources is created. The recorded data are then used to find approximate source strengths for each of the sources from which the radiated field is calculated. This distribution, however, is non-unique. (Lighthill's^{13,14} famous aeroacoustic analogy, in which the jet noise source is described mathematically as a set of quadrupoles, could be viewed as an ESM.) In an ESM, obtaining the source strengths can be accomplished with a least-squares inversion to match the measured field. For example, Shafer¹⁵ used the measured complex pressure field along a hemisphere to equivalently represent the radiation by an axial cooling fan as a collection of 19 monopoles. On the other hand, development of an ESM can also be done more empirically. For example, an oft-used model in launch vehicle noise involves defining a sound power distribution to a collection of uncorrelated sources and then applying directivity curves to the resulting radiation¹⁶⁻¹⁸. McLaughlin et al.¹⁹ also developed an uncorrelated, symmetric source distribution in examining the impact of a ground reflecting plane on model-scale jet noise. Another aeroacoustics-related ESM study is that of Holste²⁰, who applied ring-like equivalent sources to the sound radiation from engine ducts.

In developing an ESM for high-power military jet aircraft noise, one must consider the various source characteristics that should guide the development of a model. First, the jet noise source is distributed over some volume downstream of the nozzle. Second, a heated, supersonic jet appears to have an asymmetric axial source distribution, with a rapid onset followed by a slower decay downstream^{17,18,21,22}. Third, the noise field is partially correlated, owing to the finite correlation lengths of the turbulent structures. This has led to a two-source description of jet noise by Tam and others^{23,24}. Specifically, fine-scale turbulence results in a distribution of uncorrelated, omnidirectional sources throughout the plume, while large-scale turbulent structures produce more correlated radiation that has a preferred far-field directivity angle. Note that each of the jet characteristics changes as a function of frequency; hence, the ESM development must be treated on a frequency-by-frequency basis.

While the ESM model described subsequently accounts for the above source radiation mechanisms,

other features of jet noise not included are worth noting at the outset. First, mean-flow effects^{25,26}, which are required to properly describe the propagation of sound through the jet, are not included. Second, the ESM assumes an axisymmetric source distribution. Thus, azimuthal modes²⁷, which influence the sound radiation at high frequencies, are not modeled. A final characteristic of high-power military jet aircraft noise that is neglected explicitly in this study is that of nonlinear propagation. Gee et al.^{28,29} have shown that the far-field, noise propagation from the F-22 is nonlinear at intermediate and high engine powers. However, because nonlinear effects were most readily observed at frequencies above 1 kHz and at large propagation distances, a linearized ESM at low to moderate frequencies, close to the plume, is worthwhile.

In this paper, an ESM for the noise of a single engine of the F-22 Raptor is described. The model is based on data collected during an extensive field experiment¹⁰. Following a summary of the measurements, results of creating and applying the simple-source ESM are shown and discussed for different frequencies and engine conditions. The findings demonstrate the promise equivalent source methods hold in modeling jet noise.

2 FULL-SCALE EXPERIMENT

In July 2009, researchers at Brigham Young University and Blue Ridge Research and Consulting took extensive noise measurements in the vicinity of an F-22 Raptor at Holloman Air Force Base. The aircraft was tied down to a concrete run-up pad, and one engine was cycled through four engine power conditions: idle, intermediate, military, and afterburner. The other engine was operated at idle power. A complete description of the experiment is found in Ref. 10.

The data analyzed in this study were recorded on the rectangular array of microphones shown in Figs. 1



Fig. 1—The F22 Raptor tied down to the run-up pad with the 90-microphone array shown.



Fig. 2—Pictures of the rig holding a 5 x 18-microphone array. The rig is movable along the track and the physical center can be adjusted from 0.9 to 2.1 m (3 to 7 ft) from the ground.

and 2. The 90 microphones were 15.2 cm (6.0 in) apart and covered an aperture 0.6 m high by 2.6 m long (2 x 8.5 ft). The rig that held the microphones was positioned at ten locations along a 22.9 m (75 ft)-long track (visible in the pictures). The rig was also adjusted to three heights during the experiment, with the center of the array at 0.7, 1.3 and 1.9 m (27, 51, and 75 in). When the rig was moved to a different position for a new scan, it was positioned such that several microphones overlapped the previous scans. This overlapping, illustrated in Fig. 3, was done to establish consistency from scan to scan. When the data from the 30 scans are pieced together, they yield a 1.8 x 22.9 m (6 by 75 ft) measurement plane.

The track was moved to the different locations as illustrated in Fig. 4 by the solid black lines. The red

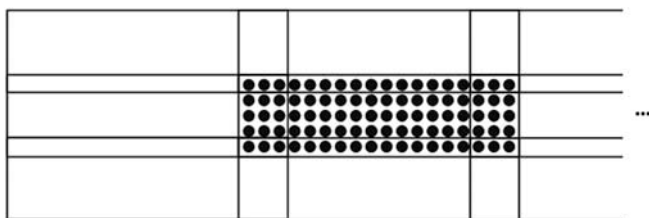


Fig. 3—The location of the microphones in the array at one scan position. The large rectangles represent the aperture covered by the rig during each scan. As the rig is moved horizontally downstream, three microphone columns overlap, and there is one microphone row overlap when the rig is moved vertically.

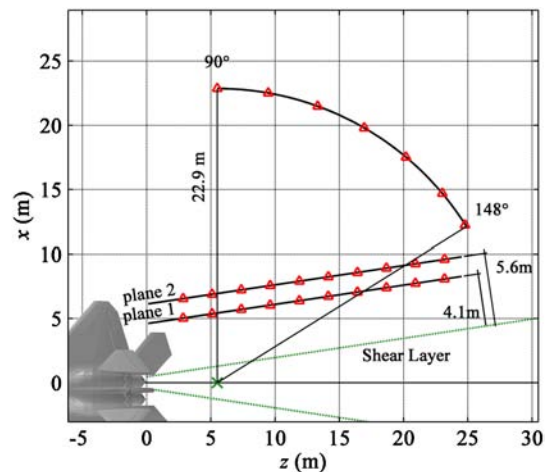


Fig. 4—Diagram of a portion of the experimental set-up for the acoustical measurements on an F-22 Raptor. A complete description of the experiment is given in Ref. 25. The triangles, each 2.3 m apart, mark the center of the microphone array for individual scans. Plane 1 is 4.1 m from the shear layer, and plane 2 is 5.6 m from the shear layer. The origin is set at ground level centered below the jet nozzle: x is the distance away from the jet plume's centerline, y is the height off the ground and z is the distance downstream from the nozzle. The green "x" refers to the estimated dominant source location and is the reference from which the angles are measured.

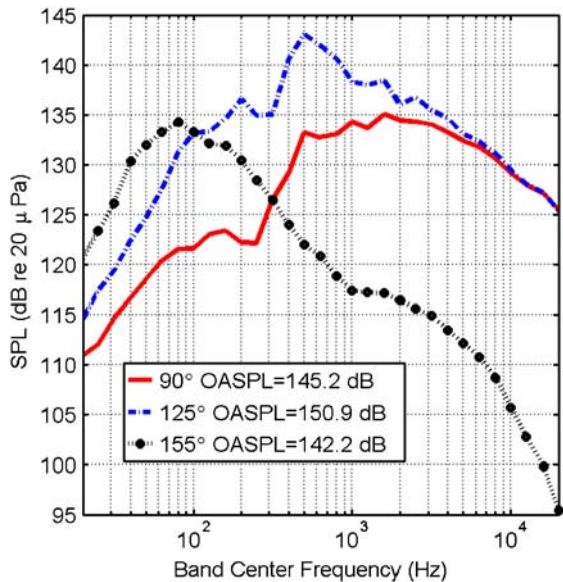


Fig. 5—One-third-octave band sound pressure level (SPL) for afterburner at three locations on plane 2: sideline (90°, relative to the nozzle inlet), the direction of the maximum level in the far field (125°), and farther downstream (155°), all at a height of $y = 1.3$ m. The overall sound pressure level for afterburner at these locations is also given.

triangles along the track indicate the locations of the center of the microphone array for subsequent measurement scans. The set of measurements obtained 4.1 m from the shear layer of the jet plume are referred to as plane 1 data, while plane 2 data come from measurements taken 5.6 m from the shear layer of the jet plume. Data along both measurement planes 1 and 2 are taken at the three heights and ten horizontal positions described in the previous paragraph. Additionally, measurements were taken along an arc, in 10° increments, where the rig was 22.9 m (75 ft) away from the estimated dominant source location²⁸, marked as a green “x” in Fig. 4. The height of the center of the array was 1.9 m (75 in) for the arc measurements. For every scan position, indicated by the triangles in Fig. 4, measurements were taken at four different engine powers: idle, intermediate, and military power and afterburner. Examples of the overall sound pressure level and the spectral content of the noise recorded for afterburner at three angles (sideline, far-field maximum radiation direction, and farther aft) and a height of 1.3 m are shown in Fig. 5. The dips in the spectra indicate the frequency-dependence of the interference between the direct and ground reflected paths.

3 MATHEMATICAL DEVELOPMENT

The main purpose of this study is to show the plausibility of using a semi-empirical, simple-source model to provide an equivalent source for jet aircraft noise. This section introduces the mathematical development behind creating this ESM. The next section shows how each component of the model contributes to the whole and compares to the measured data.

The model’s equivalent source is based on a distribution of monopoles. The arrangement and relative amplitudes of the monopoles determines the overall radiation pattern. Individually, each monopole radiates pressure omnidirectionally, and the complex pressure amplitude from a time-harmonic monopole source is

$$\tilde{P} = \frac{\tilde{A}e^{-jkR}}{R} = \tilde{A}G(\vec{r}, \vec{r}_0), \quad (1)$$

where \tilde{A} is a complex amplitude, $R = |\vec{r} - \vec{r}_0|$, k is the wave number for a given frequency and j is the complex number $\sqrt{-1}$. In this model, \vec{r}_0 is the variable source location, and \vec{r} corresponds to the microphone locations in the measured data. The pressure is also expressed in Eqn. (1) using the Green’s function, $G(\vec{r}, \vec{r}_0)$, where dependence on frequency or k is implicit.

A key factor in modeling the noise of a source in a realistic environment is to include effects of reflections, e.g. from the ground. For this ESM, the interference pattern produced by the direct noise and ground-reflected noise provides useful information about the position and distribution of the equivalent sources. Figure 6 illustrates how the direct source and its image source radiate to the measurement plane. The radiation pattern shown in Fig. 6 is the 315-Hz one-third octave band SPL along measurement plane 2 in Fig. 4. The noise along the measurement plane shows evidence of a strong interference null. The orientation of this null can be used to guide the development of an equivalent

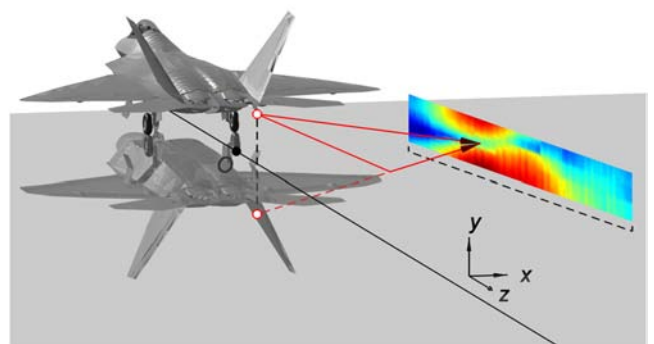


Fig. 6—A diagram showing the jet plume’s direct source and image source propagating to the measurement plane.

source based on the coherent interaction of direct and image sources. The current ESM approach is developed using line arrays of monopoles along the centerline of the jet and their images. This differs from the approach in Ref. 19, where they calculated a free-field, beam-formed source distribution for a laboratory scaled jet and applied it to the case with a ground-reflecting plane.

The addition of an image source to the monopole's complex pressure amplitude in Eqn. (1) gives

$$\tilde{P} = \tilde{A}[G(\vec{r}, \vec{r}_D) + \tilde{Q}G(\vec{r}, \vec{r}_I)], \quad (2)$$

where \vec{r}_D is the direct source vector and \vec{r}_I is the image source vector. The spherical wave reflection coefficient, \tilde{Q} , determines the amplitude and phase of the image source relative to the direct source. Although \tilde{Q} is generally a complex quantity that depends on a number of factors, including frequency, ground impedance, and angle of incidence³⁰, $\tilde{Q} = 1$ is used in this particular study, which corresponds to a rigid ground.

Equation (2) gives the complex pressure from a single monopole with a ground reflection and, with appropriate values of \tilde{A} , \vec{r}_D , and \vec{r}_I , is a "first-order" approximation to the location of the dominant equivalent source for the jet plume. A more accurate representation of the jet noise sources is obtained by including a line array of monopole sources with a smoothly varying amplitude distribution. The total complex pressure from an array of discrete monopoles over a reflecting plane is

$$\tilde{P}_T = \sum_{m=1}^N \tilde{A}_m [G(\vec{r}, \vec{r}_{D_m}) + \tilde{Q}_m G(\vec{r}, \vec{r}_{I_m})], \quad (3)$$

where \tilde{A}_m is the relative amplitude of the m^{th} monopole, and N is the total number of monopoles in the array. Although the spherical reflection coefficient \tilde{Q}_m may be different for each monopole, they are all set equal to one for the model considered here.

The amplitude distribution for the model, \tilde{A}_m , is chosen to represent observed properties of jet noise. Prior research on model-scale jets indicates that the axial strength of the sources along the jet plume do not follow a symmetric distribution (e.g., see Figs. 1, 5 and 6 in Ref. 21). Phased-array analyses on a full-scale high-power jet engine also suggest an asymmetric source distribution along the jet plume axis (cf. Fig. 11(a) in Ref. 22). In addition, computational fluid dynamics calculations by Haynes and Kenny¹⁸ for the turbulent velocity fluctuations within a large solid rocket motor plume support an asymmetric source distribution developed by Varnier¹⁷. In all three cases—the model-scale jets, the full-scale jet engine, and the large solid rocket motor plume—an

asymmetric distribution with a rapid rise and slow decay better imitates the source characteristics in the jet plume. While several well-known distributions have these characteristics, a Rayleigh distribution was chosen for this particular ESM.

A Rayleigh distribution gives the relative amplitudes of the monopoles as

$$\begin{aligned} |\tilde{A}_m(z_m, \Delta z, \sigma)| &= A_{\max} \frac{z_m - \Delta z}{\sigma^2} e^{-\frac{(z_m - \Delta z)^2}{2\sigma^2}} \\ &= A_m(z_m, \Delta z, \sigma), \end{aligned} \quad (4)$$

where z_m is the location of the m^{th} monopole, A_{\max} is the peak amplitude in the distribution, Δz is distance the peak of the distribution has been shifted downstream, and σ is the relative width of the distribution. As shown in Fig. 7, the shift distance, Δz , corresponds with the placement of the peak in the Rayleigh distribution downstream to desired location, z . In modeling the jet noise source, the relative amplitudes of the line array of monopoles at the measurement plane are controlled by the source parameters in Eqn. (4).

In addition to the asymmetry of the source distribution, another characteristic of jet noise that the model must account for is the presence of both correlated and uncorrelated noise. This is accomplished by combining two line arrays of monopoles: one correlated and one uncorrelated. For the uncorrelated source, the total squared pressure is calculated by adding up the contribution of the monopoles incoherently:

$$P_{T,u}^2 = \sum_{m=1}^N |A_{m,u} [G(\vec{r}, \vec{r}_{D_m}) + \tilde{Q}_m G(\vec{r}, \vec{r}_{I_m})]|^2, \quad (5)$$

where the subscript u denotes that this is the uncorrelated contribution to the field. In the uncorrelated line array, each monopole radiates at random with respect to the rest of the monopoles.

On the other hand, the correlated line array is assigned a fixed phase relationship among the monopole

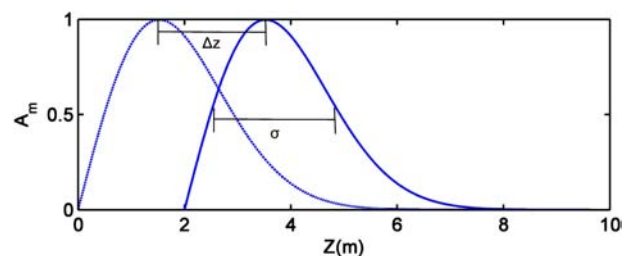


Fig. 7—A Rayleigh distribution (dotted line), which rises quickly and decays slowly, and a shifted distribution (solid line), labeled with the shift distance, Δz , and the standard deviation, σ .

amplitudes. By properly assigning the phases, it is possible to steer the sound in a desired direction. The correlated line array of monopoles is responsible for modeling the jet plume's observed peak far-field directivity of the sound radiation (at an angle θ relative to the nozzle and jet centerline)^{4,21}. To include this physical observation in the model, the phases are defined in the amplitude distribution as

$$\tilde{A}_{m,c}(z_m, \Delta z, \sigma) = A_m(z_m, \Delta z, \sigma)e^{j\varphi m}, \quad (6)$$

where φ , the phase difference, from one monopole to the next is

$$\varphi = \frac{2\pi fd \sin\theta}{c}, \quad (7)$$

and the space between the monopoles, d , is small enough to simulate a continuous source. (The sound speed is represented in Eqn. (7) by the variable c .) The far-field directivity angle θ can be obtained from analyzing a jet's far-field directivity pattern or can be included as independent parameter. The directivity angle is a function of the engine power and frequency. In the case of correlated sources, the total squared pressure is the coherent sum over the individual monopoles:

$$P_{T,c}^2 = \left[\sum_{m=1}^N \tilde{A}_{m,c} [G(\vec{r}, \vec{r}_{D_m}) + \tilde{Q}_m G(\vec{r}, \vec{r}_{I_m})] \right]^2, \quad (8)$$

where the subscript c denotes a correlated source.

The correlated and uncorrelated line arrays are combined to give the total squared pressure:

$$P_T^2 = P_{T,c}^2 + P_{T,u}^2. \quad (9)$$

This total squared pressure in Eqn. (9) is propagated via the Green's functions in Eqns. (5) and (8) to multiple observation points, which correspond to the microphone locations, and yields a planar map of the sound field to compare with the measured data. The model's parameters are adjusted to create a source that gives the least error between the model and measured data.

The error between the modeled sound field and the measured values is computed by averaging the absolute difference, on a point-by-point basis, between the model and measured data. The error is defined as

$$\text{Error} = 10 \log_{10} \left(\frac{\sum_{i=1}^{\tilde{N}} |\tilde{P}_{r,i}^2 - \tilde{P}_{m,i}^2|}{\sum_{i=1}^{\tilde{N}} \tilde{P}_{r,i}^2} \right), \quad (10)$$

where $\tilde{P}_{r,i}$ is the reference pressure from the measured data and $\tilde{P}_{m,i}$ is the model's calculated pressure at measurement location i ³¹. Because the model tends to

overestimate the depth of the interference nulls, the summation over \tilde{N} includes only points with measured levels within a 10 dB range of the maximum SPL at that plane. Not only does this reduce the contribution of the nulls to the total error, but it also emphasizes model agreement with the largest SPL values, which is our primary concern. Since the error is evaluated on a log scale as a decibel, the set of modeling parameters that yields the largest negative value of the error is the best fit.

To find a good fit between the model and the data, multiple parameters are adjusted, on a trial and error basis, to achieve the lowest possible error value. Specifically, peak source location, type of distribution, width of the distribution, relative amplitudes of the correlated and uncorrelated sources, and directivity angle are selected. For this work, the distribution is assumed to be a Rayleigh distribution, and the directivity angle, θ , is chosen based on previous far-field directivity measurements^{29,32}. The modeled line arrays are positioned on the jet plume centerline and at the height of the nozzle, about 2 m above ground. This leaves four adjustable parameters for creating an ESM that is intended to represent the jet's radiated noise at a particular frequency: the distribution's width σ , the peak location z_p and the relative amplitudes, $A_{m,c}$ and $A_{m,u}$, of the correlated and uncorrelated sources. Note that this approach utilizes the ground-reflected data to directly produce a partially correlated, asymmetric source distribution, where the work reported in Ref. 19 utilized free-field source estimates to obtain an uncorrelated, symmetric source distribution.

4 INITIAL APPLICATION OF MODEL

The implications of each step in the modeling process are now presented. As an example, the model is used to replicate the 315-Hz, one-third-octave band data measured on plane 2 while the F-22 was operating at afterburner (see Fig. 6). The parameters that characterize the equivalent source are the standard deviation and location of the peak in the distribution and the relative amplitudes of the correlated to uncorrelated sources. These are adjusted to produce a modeled source distribution with the least error according to Eqn. (10). It is beneficial to examine each property separately to see its contribution to the overall model.

The first key factor of the model is the location of the peak in the source distribution, z_p . The region of peak source strength strongly influences the location and orientation of the null caused in the sound field by the ground reflection. The peak source position z_p is the first parameter selected; it is chosen such that the

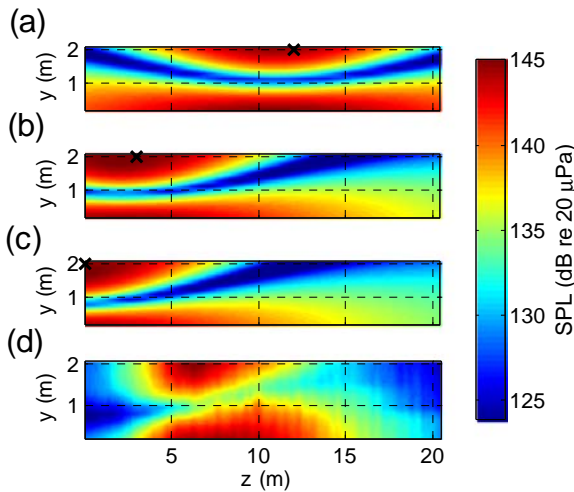


Fig. 8—SPL for the 315-Hz, one-third-octave band along measurement plane 2 resulting from a single monopole and its image source at different distances downstream: (a) 12, (b) 3, and (c) 0 m. Part (d) is the measured data for the F-22 at afterburner along plane 2.

orientation of the interference null produced by the model matches the measured data.

The effect of the peak source location on the interference pattern is illustrated in Fig. 8 using a single monopole and its image source to model the radiated field along plane 2. Figures 8(a)–(c) show the one-third-octave band SPL, centered at 315 Hz, which results from a monopole at different locations (marked by the “x”): (a) 12 m downstream, (b) 3 m downstream, and (c) the nozzle exit. The location of the monopole significantly changes the orientation of the interference null produced by the model. Figure 7(d) displays the SPL measured at afterburner over the 315-Hz one-third octave band, which also has a distinct interference null. The interference null is a dominant feature of the noise field that can be approximated with a single monopole source. Consequently, the location of the monopole that closely replicates the orientation of the nulls provides an initial guess for the downstream distance of the peak source region in the Rayleigh distribution-based model.

The remaining features of the radiated noise can be captured only if both uncorrelated and correlated sources, as expressed in Eqns. (5) and (9) are included in the ESM. Figure 9 shows the SPL computed for the one-third-octave band centered at 315 Hz for each of the components of the model separately and how they combine to produce the overall modeled field. Figure 9(a) (similar to Fig. 8(b)) shows the SPL generated by a monopole at $z_p = 2.2$ m, which best matches the alignment of the interference null in the data. The

remaining parts of Fig. 9 contain the one-third-octave band SPL maps produced by (b) the uncorrelated source alone, (c) the correlated source alone, (d) the total modeled field from the sum of (b) and (c), and (e) the measured data at afterburner. Figure 9(f) gives the absolute difference in decibel between the total modeled field and measured data at each measurement position.

The SPL map shown in Fig. 9(b) comes from Eqn. (5) for an uncorrelated line array source. The plus sign on the SPL map marks the downstream location of the peak in the Rayleigh distribution, $z_p = 2.2$ m. The uncorrelated line array’s source distribution amplitude, $A_{m,us}$, is relatively small, but the uncorrelated line array source broadens the null, compared to the monopole case, and contributes to the sideline radiation of the jet.

Equation (8) for a correlated line array source creates the SPL in Fig. 9(c), where the circle on the SPL map

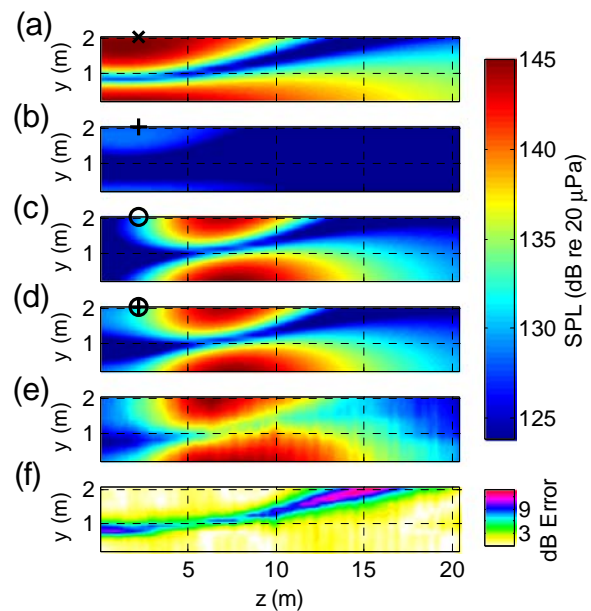


Fig. 9—SPL for the 315-Hz one-third-octave band modeled on measurement plane 2 (located 5.6 m from the shear layer of the jet plume) with a peak source location $z_p = 2.2$ m, showing the contribution of different components to the model: (a) A single monopole with its ground reflection, (b) A line array of uncorrelated monopoles, and (c) A line array of correlated monopoles with $\theta = 125^\circ$. Part (d) Shows the field from the total model, and part (e) Contains the F-22 data recorded at afterburner. Part (f) Shows the decibel error between (d) and (e).

marks the projected downstream location of the peak in the Rayleigh distribution, $z_p = 2.2$ m. The phase, φ , calculated from Eqn. (7), controls the steering of the correlated source. While the choice for θ in Eqn. (7) influences the selection of the other parameters associated with the correlated line array, for simplicity the far-field directivity angle of 125° is used based on previously measured afterburner data^{28,33}. The correlated source produces highly directional noise and contributes significantly to the downstream radiation.

The total modeled one-third-octave band SPL in Fig. 9(d) results from adding together the squared pressures from the correlated and uncorrelated sources, as in Eqn. (9), and then converting to level. A comparison of the modeled results in Fig. 9(b)–(d) to the data in Fig. 9(e) reinforces the point that both the correlated and uncorrelated portions of the model are required to match the spatial distribution of noise recorded near the F-22. The absolute value of the difference between the model's SPL (Fig. 9(d)) and the measured data's SPL (Fig. 9(e)) is defined as the decibel error and is shown in Fig. 9(f). Outside the region of the interference null there is uniformly less than 3 dB error. The areas of least agreement align with the null because the model grossly overpredicts the depth of the interference null. This overprediction could be lessened by adding a random volumetric component (without a corresponding coherent ground reflection) to the model to represent the 3-dimensional extent of the jet plume. Table 1 lists the overall error values from each part of the model when compared to the measured data: a combination of correlated and uncorrelated sources is necessary to get the least error between the modeled results and the measured data. Other than the overprediction of the null's depth, there is good agreement between the model and measured data.

Overall, the model yields an ESM for jet noise that can predict levels and SPL distributions in a large spatial region with the need to specify only a few parameters. This section has described applying the model to one set of the measured data to create an equivalent source. However, for the resulting equivalent source to be considered representative of the noise sources within the jet plume, it needs to be able to predict the radiated field at other locations. Evidence that this, in fact, occurs as well as the further application of the model

to different frequencies and engine powers is provided in the next section.

5 MODEL RESULTS

The initial application of a semi-empirical, simple-source model as an equivalent source for jet noise was presented in the previous section for one subset of the F-22 data: the 315 Hz one-third octave-band levels at measurement plane 2 for afterburner engine power. This section focuses on how the model performs for different propagation distances, frequencies, and engine conditions.

5.1 Benchmark Tests

The equivalent source parameters chosen in the previous section are now propagated to other measurement planes to test its accuracy at different distances. By applying the parameters chosen to match the data along plane 2, referred to as the construction plane, to predict the field both closer to (plane 1) and farther from (the arc) the source, the capability of the model to yield equivalent source characteristics that can be used to predict the fields at locations other than the original construction plane is demonstrated.

Measurement plane 1 is parallel to the shear layer of the jet plume and to plane 2, as shown in Fig. 4, and is closer to the jet plume (3.8 m offset) than plane 2 (5.6 m offset). Figure 10(a) shows the results when the modeling parameters obtained for plane 2 are instead propagated to plane 1. Figure 10(b) is the measured data at plane 1, and Fig. 10(c) displays the decibel error between the modeled results and the data. Figure 10 shows that the ESM parameters chosen to match the data on plane 2 produce SPL values that agree with the data on plane 1 to within 3 dB, except near the interference nulls, as explained previously.

The equivalent source model also needs to be able to reproduce the SPL on measurement planes that are farther from the source than the construction plane (plane 2). For the F-22 experiment, the locations used for comparison are along an arc 22.9 m (75 ft) from the estimated dominant source location in the jet plume. For other analytical/computational methods, outward propagation of the sound is simpler, but for this model any errors in the selection of the source

Table 1—Error in decibels [as defined in Eqn. (10)] between each part of Fig. 9 (a)–(d) and (e) the measured data.

Fig. 9	(a)	(b)	(c)	(d)
Source Type	Single Monopole	Uncorrelated Line Array	Correlated Line Array	Total Model
Error (dB)	– 2.7	– 0.09	– 6.0	– 6.2

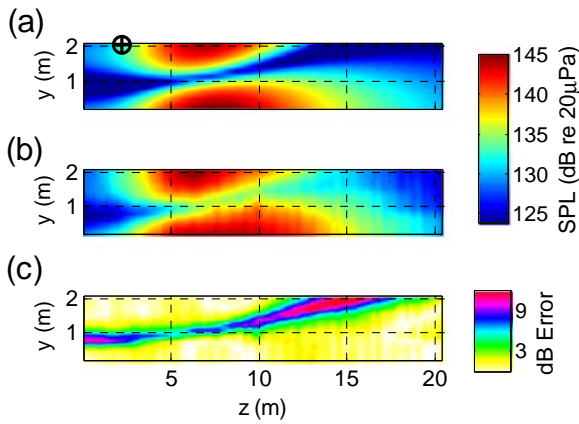


Fig. 10—One-third-octave-band SPL for 315 Hz, along measurement plane 1 (located 3.8 m from shear layer of the jet plume) where (a) is the total modeled field and (b) is the data recorded at afterburner. Part (c) displays the decibel error between them.

parameters at the construction plane are emphasized at this greater distance; in particular, any errors in the directivity angle θ would be evident. Figure 11 shows the three measurement locations: plane 1, plane 2 and the arc. Figure 11(a) contains the model's

predictions and (b) displays the measured data. Table 2 shows the total error values at each of the measurement planes. Although the construction plane has the least error, the fields predicted at other locations still prove to be reasonable. The SPL along the top of the arc at 315 Hz is displayed in Fig. 12(b) and shows that the amplitude of the modeled noise rolls off correctly in both the upstream and downstream directions. The ability to predict the field closer to and farther from the jet confirms that the angle of 125° used from the known far-field directivity pattern²⁹ for the afterburner engine condition is adequate. This example indicates the flexibility of the model in predicting the spatial variation of the noise levels at different locations in the near and mid fields.

5.2 Other Frequencies

The flexibility of the model is further demonstrated by showing how the model works for additional frequencies. The results of equivalent source modeling for two other frequencies (125 and 800 Hz), using the same method outlined above, are compared to the corresponding afterburner data on plane 2. The parameters of the modeled sources, such as the width of the source distribution, its peak location, and the relative amplitudes of the correlated and uncorrelated sources, depend on frequency via the Green's function, as shown in Eqns.(5) and (8).

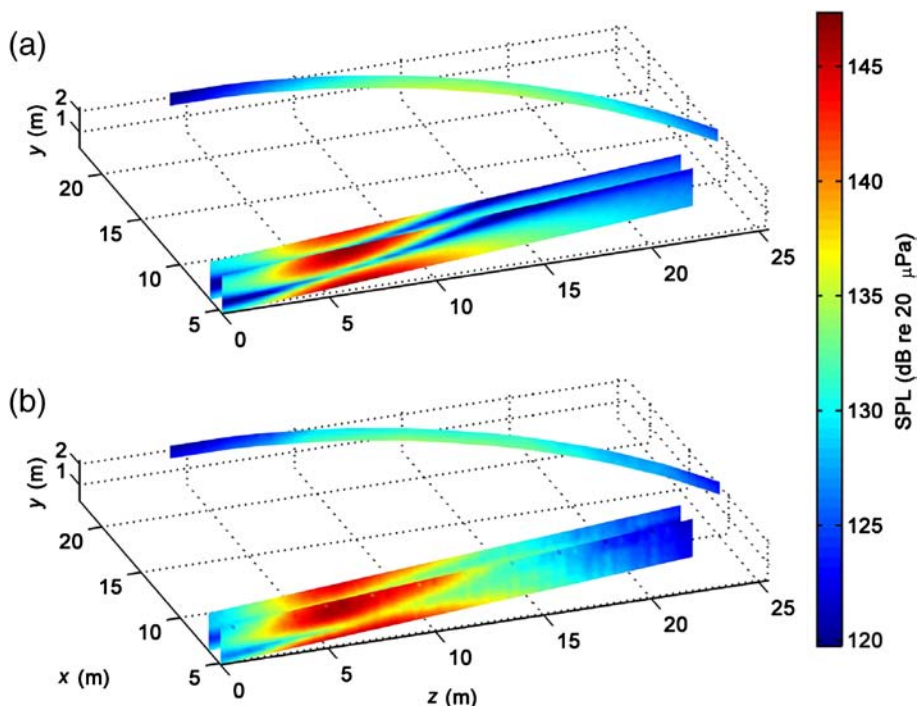


Fig. 11—A 3-D plot to show the 315-Hz one-third-octave band SPL on multiple measurement planes and agreement between model and data at various distances: (a) Model using source parameters chosen on plane 2 and (b) Measured data at afterburner.

Table 2—Error in decibels [as defined in Eqn. (10)] at all three measurement planes for afterburner.

Measurement plane	1	2	Arc
Error at 125 Hz (Fig. 14)	-5.9	-5.8	-6.6
Error at 315 Hz (Fig. 11)	-3.7	-6.1	-4.2
Error at 800 Hz (Fig. 16)	-3.2	-4.4	-4.3

Figure 13 shows the SPL for the one-third-octave band centered at 125 Hz along plane 2 from (a) the model with $z_p = 4.9$ m and (b) the measured data at afterburner engine power. At 125 Hz, there are no nulls in the measured noise field. Nevertheless, Fig. 13(a) shows that the model is still able to reproduce this radiation pattern to within 3 dB at most locations. Figure 14 shows the corresponding 3-dimensional maps of the SPL generated by the model in part (a) and measured during the experiment in part (b). A closer look at the actual and predicted values for the highest microphone along the arc is shown in Fig. 12(a). The ability of the model to match the 125-Hz data is significant because 125 Hz is near the peak in the broadband noise spectrum of the F-22 at afterburner in the maximum-

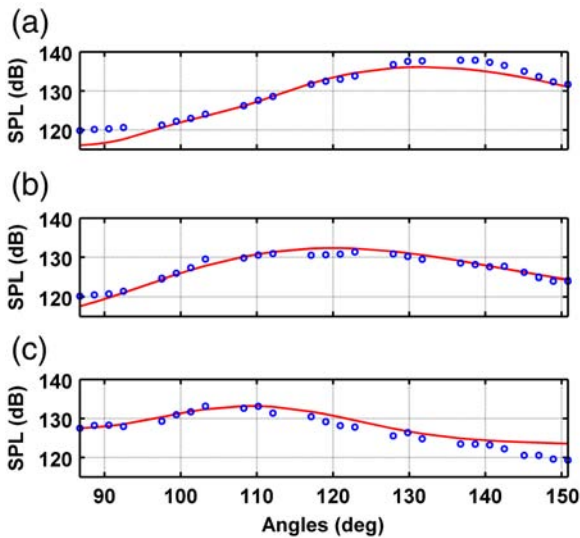


Fig. 12—Comparison of the afterburner data (blue dots) at (a) 125, (b) 315, and (c) 800 Hz recorded on microphones along the top of the field array 22.9 m (75 ft) from the jet and the ESM prediction (red lines) from parameters obtained by matching the data on plane 2. The angles are computed from the estimated dominant source region, shown as an “x” in Fig. 4.

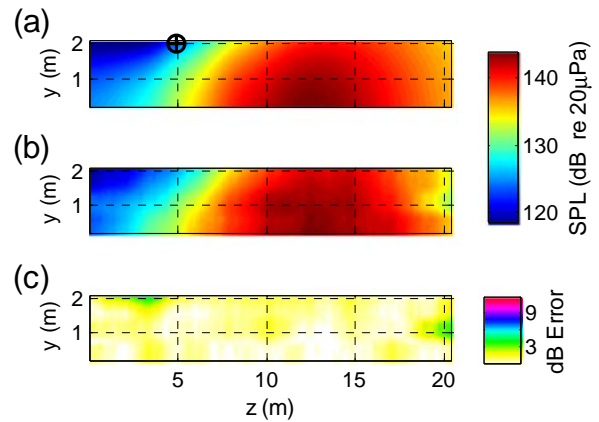


Fig. 13—SPL for the 125-Hz one-third-octave band along measurement plane 2 for (a) the model with $z_p = 4.9$ m and (b) the measured data at afterburner engine power. Part (c) displays the decibel error between them.

radiation direction ($\theta = 130^\circ$)^{12,28}. Consequently the value of $z = 4.9$ m used to model the field gives a good indication of the location of the dominant source region within the jet plume.

Figure 15 shows the SPL for the one-third octave band centered at 800 Hz along plane 2 where (a) is the model with $z_p = 0.7$ m and $\theta = 120^\circ$ and (b) the measured data at afterburner, and (c) displays the decibel error between them. Figure 15 gives evidence that the model can reproduce the respective locations and shapes of multiple nulls, except that the model produces greater levels downstream at this higher frequency than what are seen in the data. This could be due to the importance of azimuthal modes at high frequencies relative to the assumed axisymmetry²⁷. The results of using the source parameters selected for plane 2 to predict the noise field at other locations are shown in Fig. 16. The sound field generated by the model is shown in Fig. 16(a), while the afterburner data are displayed in Fig. 16(b), and the values across the top of the arc are displayed in Fig. 12(c). The error values for the different planes are listed in Table 2. As in the 315-Hz case, the source characteristics chosen for plane 2 provide an equivalent representation of the jet noise sources that capture the primary features of the field both closer to and farther from the jet, with the exception of the longer radiation tails produced by the model at 800 Hz as seen on both plane 1 and plane 2.

5.3 Other Engine Conditions

The next variable to explore is how the model performs for different engine powers. This section shows

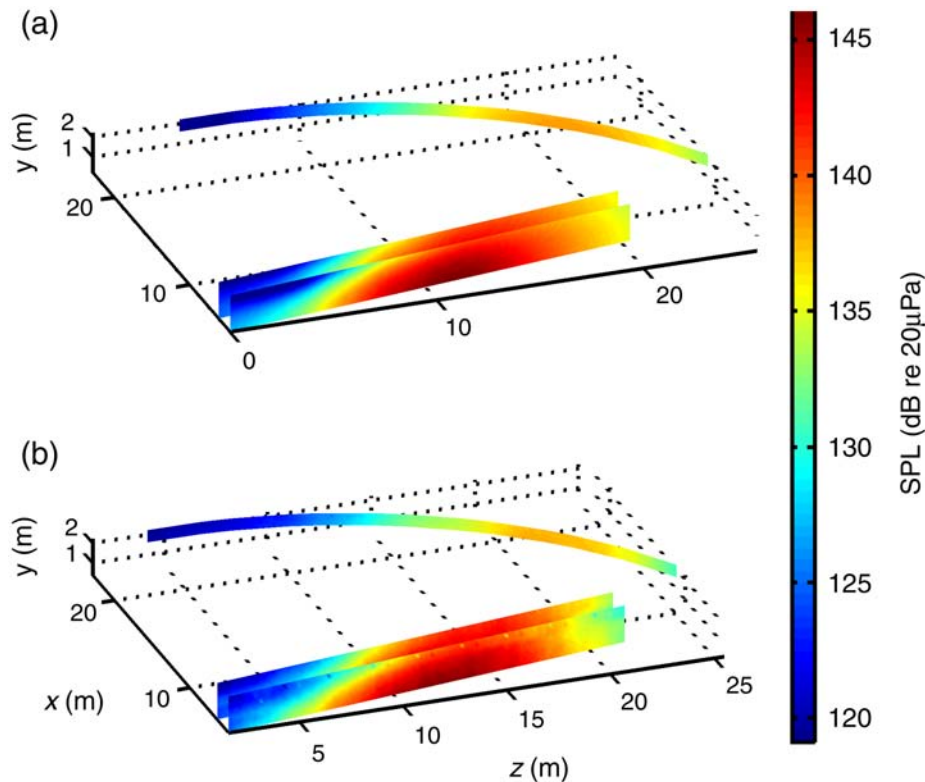


Fig. 14—A 3-dimensional plot to show the 125-Hz one-third-octave band SPL at on multiple measurement planes where (a) is the model with $z_p = 4.9$ m and (b) is the measured data afterburner.

the model results for the 315-Hz one-third-octave-band SPL data at military and idle engine powers.

Figure 17 contains the SPL for the one-third-octave band centered at 315 Hz along plane 2 of (a) the model with $z_p = 2.1$ m and (b) the measured data at military engine power, while part (c) contains the decibel error between them. The data for military power (in Fig. 17(b))

and afterburner (in Fig. 9(e)) are similar, except for a few things: the SPL for the military power is several decibels lower and the peak amplitude area is farther upstream and does not extend as far downstream. The far-field directivity angle θ was 130° ²⁹. The total error for the case of military power (shown in Table 3) is similar to the afterburner case.

Figure 18 shows the SPL for the one-third-octave band centered at 315 Hz for (a) the model with $z_p = 1.5$ m and (b) the measured data at the idle engine power, while (c) displays the decibel error between them. The levels recorded in the idle-power data are much lower and are concentrated at shallower angles than for higher engine powers. The peak source location required to match the data at idle power is closer to the nozzle and the modeled sound field is generated solely by uncorrelated sources, which appear to be responsible for the sideline radiation. Similar to the 800-Hz, afterburner case, the model for the 315-Hz case at idle produces much longer tails than what are seen in the data. This overprediction appears to occur when the modeled uncorrelated source dominates the radiated noise. While this discrepancy is reflected in the higher error value in Table 3, as compared to afterburner and military power, the match is still within 2 dB in the regions of largest amplitude.

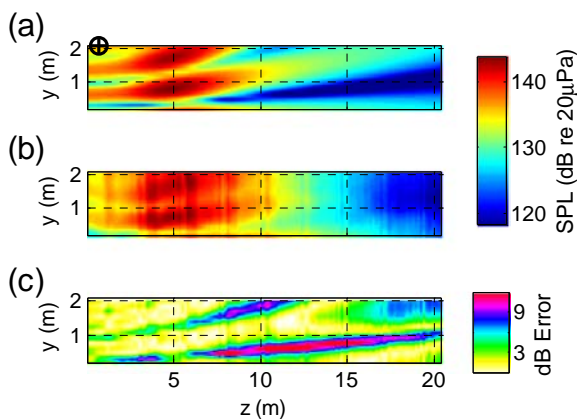


Fig. 15—SPL for the 800-Hz one-third-octave band along measurement plane 2 for (a) the model with $z_p = 0.7$ m and (b) the measured data at afterburner engine power. Part (c) displays the decibel error between them.

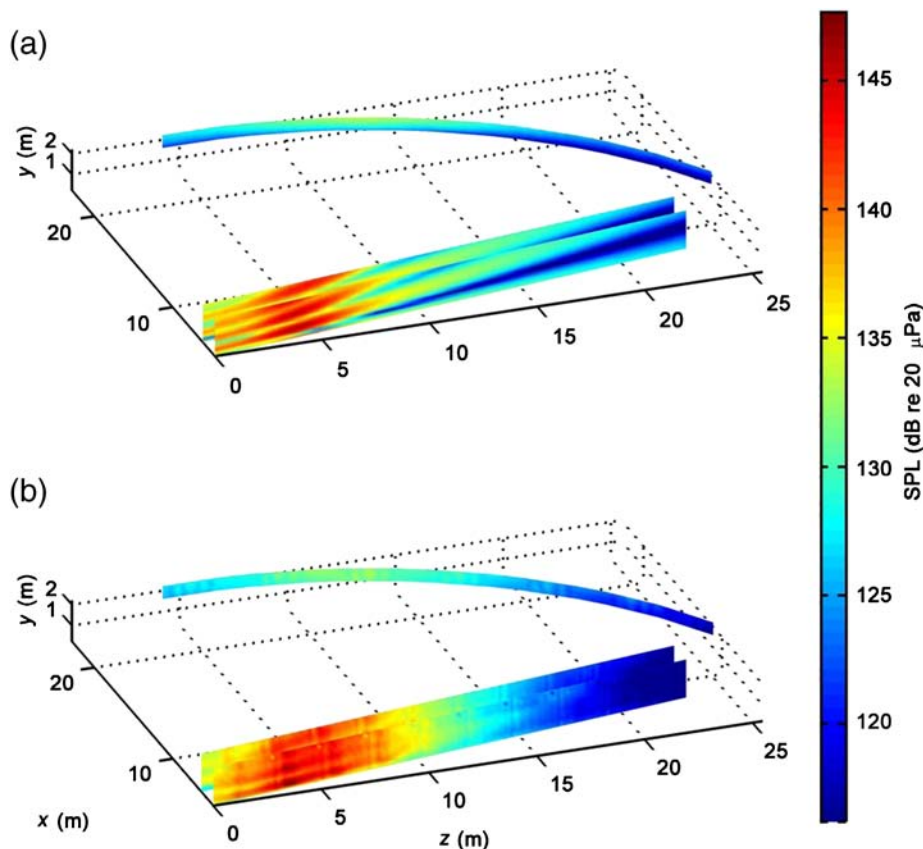


Fig. 16—A 3-dimensional plot to show the 800-Hz one-third-octave band SPL at on multiple measurement planes where (a) is the model with $z_p = 0.7$ m and (b) is the measured data afterburner.

5.4 Observations

Overall, this model is able to create equivalent source distributions of jet noise for a variety of frequencies, offset distances, and engine powers. The resulting equivalent source distributions vary with frequency and engine condition. Figure 19 shows the correlated and uncorrelated source distributions used in the ESM for the different frequencies shown in Figs. 9 through 16. Figure 20 shows the correlated and uncorrelated source distributions used in the ESM for the engine powers shown in Figs. 9, 17 and 18.

Specifically, Fig. 19 shows how the peak in the amplitude distribution moves upstream and the distribution narrows as frequency increases. The correlated source is the dominant source at the lower frequencies (125 and 315 Hz) due to the coherent sum in Eqn. (8), while the uncorrelated source is dominates the noise at 800 Hz. Both the shift in peak location towards the nozzle and the increase in the relative amplitude of the uncorrelated sources increase as frequency increases indicate more sideline radiation at higher frequencies.

The change in the location of the peak source region z_p with frequency agrees with theory and other

experiments. Various phased-array methods applied to jet noise have seen a trend for the maximum source region to move upstream and get narrower as frequency

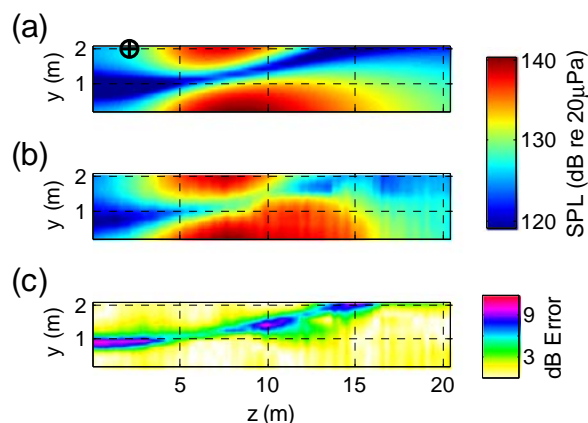


Fig. 17—SPL for the 315-Hz one-third-octave band centered along measurement plane 2 of (a) the model with $z_p = 2.1$ m and (b) the measured data at military engine power. Part (c) displays the decibel error between them.

Table 3—Error in decibels [as defined in Eqn. (10)] for 315-Hz case for afterburner, military power and idle engine conditions at measurement plane 2.

Engine Condition	AB (Fig. 8)	Mil (Fig. 17)	Idle (Fig. 18)
Error (dB)	-6.1	-6.7	-4.9

increases^{33,34}. While phased-array results are related to the specified observation direction, the overall equivalent source from the current model captures this feature: higher-frequency noise requires a peak source location closer to the nozzle and a narrower distribution, while the lower frequency noise requires a wider distribution and peak source region located farther downstream. The change in peak source location with frequency also agrees with underlying principles of Tam’s two-source model regarding how turbulent structures in the jet generate noise. The fine-scale turbulent structures form immediately aft of the nozzle and contribute primarily high-frequency noise that is omnidirectional. Flow instabilities cause large-scale turbulent structures to grow and spread out as they move downstream that cause directional low-frequency noise^{21,23,24}. The semi-empirical, simple-source model presented in this paper captures these key traits of this physical system over a range of frequencies.

In addition to the change in the distributions with frequency, the width and location of the peak of the distribution also change with engine condition. Figure 20 shows that the location of the peak source region moves upstream with decreasing engine power. Also, the relative amplitude of the correlated source to the

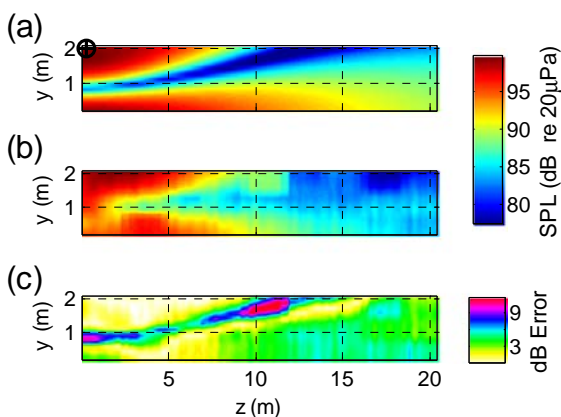


Fig. 18—SPL for the one-third-octave band centered at 315 Hz along measurement plane 2 of (a) the model with $z_p = 1.5$ m, (b) the measured data at idle engine power, and (c) the decibel error between them.

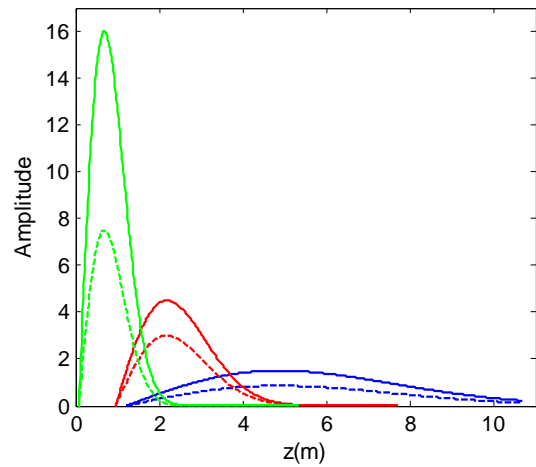


Fig. 19—Correlated (dashed) and uncorrelated (solid) equivalent source distributions at afterburner for the 125 (blue), 315 (red), and 800 Hz (green). (Note that although the correlated amplitude is lower, its overall contribution to the squared pressure is greater at 125 and 315 Hz.)

uncorrelated source decreases with decreasing engine power to the point that the equivalent source distribution chosen for idle engine power consists only of uncorrelated sources. Regarding distribution width, the military and afterburner equivalent source distributions are both more extended than for idle. However, the distribution for afterburner condition has higher amplitude, and the peak is slightly farther downstream,

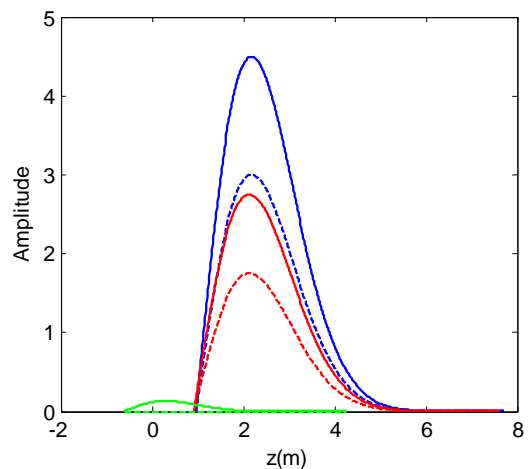


Fig. 20—Correlated (dashed) and uncorrelated (solid) equivalent source distributions at 315 Hz for three engine powers: idle (green), military (red), and afterburner (blue).

reflecting the increase in power. The shift is related to the increase in jet velocity caused by the increased temperature at afterburner.

6 CONCLUSIONS

In summary, this equivalent source model (ESM) is able to approximate jet-noise phenomena measured along a planar aperture. The combination of a correlated and an uncorrelated line arrays of simple sources with Rayleigh-distributed amplitudes reproduce the sound radiated from an F-22 Raptor to within 3 dB, except near the interference nulls. More importantly, the ESM parameters chosen to match the data on one measurement plane also give reasonable results for the radiated field at additional distances from the jet.

The characteristics of the ESMs that best match the data agree with previously observed features of jet noise^{21,22}. Radiation at lower frequencies and higher engine powers requires a wider distribution of sources with the peak source region located several nozzle diameters downstream and are dominated by correlated sources. Conversely, radiation at higher frequencies and lower engine powers are dominated by uncorrelated sources, have narrower distributions and are concentrated closer to the nozzle. The necessity of using a combination of correlated and uncorrelated sources to reproduce jet noise agrees with the underlying principle of Tam's two-source theory^{23,28}. The contraction and movement upstream of the source region predicted by the model also agrees with various phased-array measurements^{33,34}.

This simple-source ESM presented in this paper has a few features that limit its ability to make predictions about the turbulent source structures in the jet plume. First, the model assumes a line array of sources when in fact jet noise is a volume source. Secondly, it assumes a perfectly coherent ground reflection. Both of these assumptions contribute to the model over predicting of the depth of the interference nulls. The depth of the interference nulls can be decreased by including a random volumetric source to better simulate the size and chaotic nature of the jet plume. In modeling the jet as a volumetric source, the azimuthal modes could be included, which would likely improve the agreement at higher frequencies²⁷. Third, currently, the model includes the assumption that the equivalent source radiates from the center line. The model could be adapted to shift the location of the equivalent sources to the shear layer, which would allow comparison with the phased-array experiments reported by Tam et al.,²³ or mean-flow effects could be added to the equivalent sources along the centerline^{25,26}. Finally, another investigation, currently underway, involves optimizing the

search for the parameters in the ESM model as an inverse problem. In addition, such an optimization algorithm could include the capability of finding equivalent source amplitude distributions in a more general and rigorous manner.

7 ACKNOWLEDGMENTS

The authors gratefully acknowledge funding from the Air Force Research Laboratory through the SBIR program and support through a Cooperative Research and Development Agreement (CRADA) between Blue Ridge Research and Consulting LLC, Brigham Young University, and the Air Force. We would also like to thank the reviewers for the insightful comments and recommendations.

8 REFERENCES

1. J. Bridges and M. Wernet, "Measurements of the aeroacoustic sound source in hot jets", NASA/TM – 2004-212508, NASA Glenn Research Center, (2004).
2. V. Fleury, C. Bailly, E. Jondeau, M. Michard and D. Juvé, "Space-time correlations in two subsonic jets using dual particle velocimetry measurements", *AIAA J.*, **46**, 2498–2509, (2008).
3. C. Bailly, P. Lafon and S. Candel, "Subsonic and supersonic jet noise predictions from statistical source models", *AIAA J.*, **35**, 1688–1696, (1997).
4. C.K.W. Tam, N.N. Pastouchenko and K. Viswanathan, "Extension of the near acoustic field of a jet to the far field", *Procedia IUTAM*, **1**, 9–18, (2010).
5. J.R. Stone and F.J. Montegani, "An improved prediction method for the noise generated in flight by circular jets", *J. Acoust. Soc. Am.*, **67**, S4, (1980).
6. K. Viswanathan, "Mechanisms of jet noise generation: Classical theories and recent developments", *Int. J. of Aeroacoustics*, **8**, 355–407, (2009).
7. A. Bassetti, M.J. Fisher and C.L. Morfey, "A semi-empirical model of jet noise prediction in the geometric near field", *AIAA paper 2004-2831*, (2004).
8. M. Lee and J.S. Bolton, "Source characterization of a subsonic jet by using near-field acoustical holography", *J. Acoust. Soc. Am.*, **121**, 967–977, (2007).
9. A.T. Wall, K.L. Gee, M.D. Gardner, T.B. Neilsen and M.M. James, "Near-field acoustical holography applied to high-performance jet aircraft noise", *Mtgs. Acoust.*, **9**, 040009, (2011).
10. A.T. Wall, K.L. Gee, M.M. James, K.A. Bradley, S.A. McInerney and T.B. Neilsen, "Near-field noise measurements of a high-performance military jet aircraft", *Noise Control Engr. J.*, **60**(4), 421–434, (2012).
11. M. Ochmann, "The source simulation technique for acoustic radiation problems", *Acustica*, **81**, 512–527, (1995).
12. N.P. Valdivia and E.G. Williams, "Study of the comparison of the methods of equivalent sources and boundary element methods for near-field acoustic holography", *J. Acoust. Soc. Am.*, **120**, 3694–3705, (2006).
13. M.J. Lighthill, "On Sound generated aerodynamically. Part 1. General Theory", *Royal Soc. London*, **211**, 564–587, (1952).
14. F. Farassat, M.J. Doty and C.A. Hunter, "The acoustic analogy – A powerful tool in aeroacoustics with emphasis on jet noise prediction", *AIAA paper 2004-2872*, (2004).
15. B.M. Shafer, "Error sensor placement for active control of an axial cooling fan", MS thesis, Brigham Young University, (2007).
16. K.M. Eldred, "Acoustic Loads Generated by the Propulsion System", *NASA SP-8072*, (1971).

17. J. Varnier, "Experimental study and simulation of rocket engine free jet noise", *AIAA J.*, **39**, 1851–1859, (2001).
18. J. Haynes and R. Kenny, "Modifications to the NASA SP-8072 Distributed Source Method II for Ares I Lift-Off Environment Predictions", *AIAA paper 2009-3160*, (2009).
19. D.K. McLaughlin, C.W. Kuo, and D. Papamoschou, "Experiments on the Effect of Ground Reflections on Supersonic Jet Noise", *AIAA paper 2008-22*, (2008).
20. F. Holste, "An Equivalent Source Method for Calculation of the Sound Radiated from Aircraft Engines", *J. Sound Vibr.*, **203**, 667–695, (1997).
21. C.K.W. Tam, N.N. Pasouchenko and R.H. Schlinker, "Noise source distribution in supersonic jets", *J. Sound Vibr.*, **291**, 192–201, (2006).
22. R.H. Schlinker, S.A. Lijenberg, D.R. Polak, K.A. Post, C.T. Chipman and A.M. Stern, "Supersonic Jet Noise Source Characteristics & Propagation: Engine and Model Scale", *AIAA paper 2007-3623*, (2007).
23. C.K.W. Tam, K. Viswanathan, K.K. Ahuja, and J. Panda, "The sources of jet noise: experimental evidence", *J. Fluid Mech.*, **615**, 253–292, (2008).
24. C.K.W. Tam, M. Golebiowski and J.M. Seiner, "On the Two Components of Turbulent Mixing Noise from Supersonic Jets", *AIAA paper 96-1716*, (1996).
25. U. Michel, "The role of source interference in jet noise", *AIAA paper 2009-3377*, (2009).
26. S. A. Karabasov, "Understanding jet noise", *Phil. Trans. Roy. Soc.*, **A368**, 3593–3608.
27. H. Vold, P. Shah, P. Morris, Y. Du and D. Papamoschou, "Axisymmetry and azimuthal modes in jet noise", *AIAA paper 2012-2214*, (2012).
28. K.L. Gee, V.W. Sparrow, M.M. James, J.M. Downing, C.M. Hobbs, T.B. Gabrielson, and A.A. Atchley, "The role of nonlinear effects in the propagation of noise from high-power jet aircraft", *J. Acoust. Soc. Am.*, **123**, 4082–4093, (2008).
29. K.L. Gee, V.W. Sparrow, M.M. James, J.M. Downing, C.M. Hobbs, T.B. Gabrielson, A.A. Atchley, "Measurement and prediction of noise propagation from a high-power jet aircraft", *AIAA J.*, **45**, 3003–3006, (2007).
30. E. M. Salomons, *Computational Atmospheric Acoustics*, Kluwer Academic Publishers, Norwell, MA, (2001), pp. 123–137.
31. J. Hald, "Basic Theory and properties of statistically optimized near-field acoustical holography", *J. Acoust. Soc. Am.*, **125**, 2105–2120, (2009).
32. Air Force Research Laboratory, *NOISEFILE Database*, Wright-Patterson AFB, OH, (2003).
33. D. Papamoschou, "Imaging of directional distributed noise sources," *14th AIAA/CEAS Aeroacoustics Conference*, (2008)
34. S.S. Lee and J. Bridges, "Phased-array measurements of single flow hot jets", *AIAA paper 2005-2842*, (2005).